Enhancing the Imaging and Biosafety of Upconversion Nanoparticles through Phosphonate Coating

Ruibin Li,[†,⊥] Zhaoxia Ji,[‡,⊥] Juyao Dong,[§] Chong Hyun Chang,[‡] Xiang Wang,[‡] Bingbing Sun,[†] Meiying Wang,[†] Yu-Pei Liao,[†] Jeffrey I. Zink,[‡,§] Andre E. Nel,[*,†,‡] and Tian Xia[*,†,‡]

[†]Division of NanoMedicine, Department of Medicine, University of California Los Angeles, 10833 Le Conte Avenue, Los Angeles, California 90095, United States, [‡]California NanoSystems Institute, University of California Los Angeles, 570 Westwood Plaza, Los Angeles, California 90095, United States, and [§]Department of Chemistry & Biochemistry, University of California Los Angeles, 607 Charles E. Young Drive East, Los Angeles, California 90095, United States. [⊥]R. Li and Z. Ji equally contributed to this work.

ABSTRACT Upconversion nanoparticles (UCNPs), which are generated by doping with rare earth (RE) metals, are increasingly used for bioimaging because of the advantages they hold over conventional fluorophores. However, because pristine RE nanoparticles (NPs) are unstable in acidic physiological fluids (*e.g.*, lysosomes), leading to intracellular phosphate complexation with the possibility of lysosomal injury, it is important to ensure that UCNPs are safely designed. In this study, we used commercially available $NaYF_4$:Er/Yb UCNPs to study their stability in lysosomes and simulated lysosomal fluid. We demonstrate that phosphate complexation leads to $REPO_4$ deposition on the particle surfaces and morphological transformation. This leads to a decline in upconversion fluorescence efficiency as well as inducing pro-inflammatory effects at the cellular level and in the intact lung. In order to preserve the imaging properties of the UCNPs as well as improve their safety, we experimented with a series of phosphonate chemical moieties to passivate particle surfaces through the strong coordination of the organophosphates with RE atoms. Particle screening and physicochemical characterization revealed that ethylenediamine tetra(methylenephosphonic acid) (EDTMP) surface coating provides the most stable UCNPs, which maintain their imaging intensity and do not induce pro-inflammatory effects *in vitro* and *in vivo*. In summary, phosphonate coating presents a safer design method that preserves and improves the bioimaging properties of UCNPs, thereby enhancing their biological use.

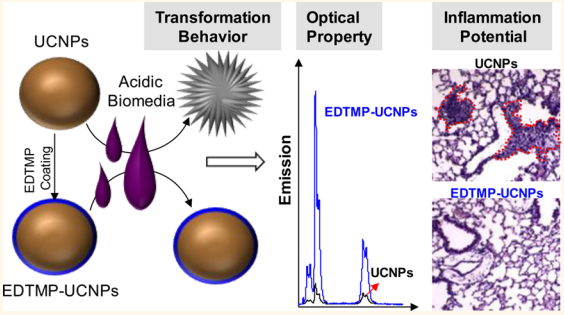

KEYWORDS: nanotoxicity · surface coating · fluorescence quenching · functionalization · lysosome · cell uptake

Rare earth (RE) metals are commonly used for the synthesis of upconversion nanoparticles (UCNPs), which can be used for biological applications.[1−5] UCNPs are traditionally synthesized as guest−host systems, in which trivalent lanthanide ions (the guest) are dispersed in an appropriate dielectric RE-based host lattice.[6,7] Sequential absorption of multiple low-energy photons by the ladder-like energy levels of the lanthanide dopants leads to the production of higher energy anti-Stokes luminescence.[8] This allows the emission wavelength to be tuned from near-infrared (NIR) to visible through to the UV range, depending on the type of lanthanide being used.[9−13] The use of optical properties together with the high resistance to photobleaching and photochemical degradation allows lanthanide-doped UCNPs to be considered as promising new bioimaging agents for advanced accomplishments, such as single-molecule tracking, multiplexed labeling, and deep tissue imaging.[14−20] While to date no serious toxicity has been observed during the use of UCNPs in organisms such as *Caenorhabditis elegans*,[2,21] zebra fish,[22] and rodent studies,[16,23−25] we are aware of the problems caused by Gd-based MRI agents in renal failure patients, where these reagents can lead to nephrogenic systemic fibrosis (NSF).[26,27] Moreover, there is documentation of the occurrence of an occupational lung disease in RE miners or workers exposed to RE materials (*e.g.*, during polishing activity).[28] Against this background, it is important to consider early stage safer design strategies for the biological implementation of UCNPs as imaging agents.

* Address correspondence to txia@ucla.edu (T. Xia), Anel@mednet.ucla.edu (A. Nel).

Received for review January 21, 2015 and accepted March 1, 2015.

Published online March 02, 2015
10.1021/acsnano.5b00439

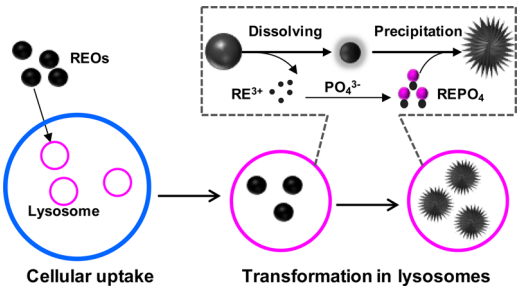

Scheme 1. Transformation of RE particles in an acidic biological environment. RE nanoparticles taken up into lysosomes undergo dissolution in the acidic lysosomal environment and shed RE ions that bind to cellular phosphate residues, which precipitate on the particle surface to form urchin-shaped $REPO_4$ structures.

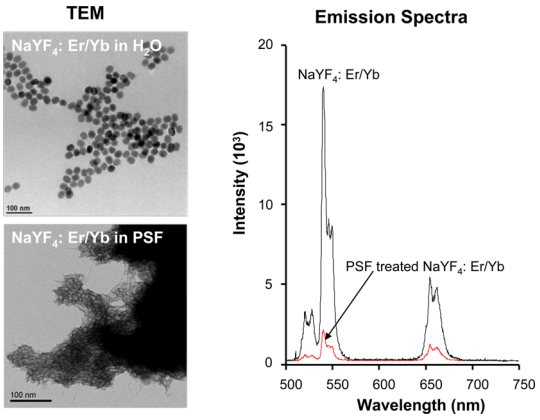

Figure 1. Transformation and emission spectrum of $NaYF_4$: Er/Yb nanoparticles exposed to PSF. NPs were dispersed in PSF for 24 h at a concentration of 100 μg/mL. Particle suspensions were centrifuged at 100 000 rpm/min for 1 h to collect the pellets. After washing three times with DI H_2O, the pellets were resuspended in DI H_2O. Untreated and PSF-treated particle suspensions were used to study the particle morphology by TEM, as well as obtaining the emission spectra at an excitation wavelength of 980 nm.

Relevant background to this study is the recent demonstration that rare earth oxide (REO) nanoparticles are unstable in acidic cellular environments such as lysosomes, where the release of RE ions leads to complexation of critical phosphates that precipitate as insoluble $REPO_4$ on the particle surfaces (Scheme 1).[29] This leads to morphological transformation into urchin-shaped structures, which can deplete structurally important lipids and proteins of their phosphate groups, leading to lysosomal membrane damage, cathepsin B release, and initiation of pro-inflammatory effects.[29,30] An example includes activation of the NLRP3 inflammasome, which is responsible for IL-1β production, chronic pulmonary inflammation, and fibrosis.[29] This could result in RE-induced pneumoconiosis in polishers and miners,[28] while Gd-based imaging agents could induce NSF in people with chronic renal failure, metabolic acidosis, and hyperphosphatemia.[27,31,32] While there are no reports of similar UCNP adverse effects to date, we have observed that Er- and Yb-doped $NaYF_4$ as well as $La(OH)_3$ UCNPs do form mesh- or urchin-like structures in the lysosomes of myeloid cells and macrophages. Moreover, there is a reduction of the fluorescence intensity of UCNPs in macrophages recovered from the liver.[25,33] Thus, the transformation of RE materials under specific biological conditions could lead to the generation of a biological hazard as well as a decline in their imaging qualities.

In this article, we set out to use our expertise of the adverse impact of RE nanoparticles on household cellular phosphates to attempt to design safer UCNPs, with preserved imaging capabilities. Key to the accomplishment of safer design is the prior observation that phosphate complexation to RE nanoparticle surfaces at neutral or physiological pH can prevent subsequent particle transformation under acidic conditions.[29] This led us to consider a series of phosphonate chemical groups for a coating procedure that prevents biological hazards while, at the same time, maintaining imaging quality. We settled on ethylenediamine tetra-(methylenephosphonic acid) (EDTMP) as the most effective phosphonate coating agent to passivate UCNP surfaces. This safer design procedure prevents the transformation of UCNPs under biological conditions, in addition to preventing their fluorescence quenching. The phosphonate coating also reduced the pro-inflammatory effects of UCNPs *in vitro* and *in vivo*.

RESULTS

Chemical and Morphological Transformation of UCNPs Affects the Imaging Quality of UCNPs. Since an acidic biological environment affects the stability and chemical composition of RE nanoparticles, a $NaYF_4$-based UCNP, coated with oleic acid, was used to determine what effect an acidic lysosomal environment may have on particle composition and imaging qualities.[34] $NaYF_4$:Er/Yb particles with a primary size of 22 nm and a positive surface charge (zeta potential of +16.4 mV in DI H_2O) were selected for abiotic and biotic experimentation (Table S1). Because of the oleic acid coating, the particles agglomerated in DI H_2O to a hydrodynamic size of 212 nm but were dispersed to 39 nm in the presence of proteins in the cell culture media. However, in the presence of the acidic phagolysosomal simulated fluid (PSF, pH 4.5) for 24 h, the spherical particles transformed into mesh-like structures as determined by TEM analysis (Figure 1). These transformed particles showed a loss of crystallinity as determined by X-ray diffraction (XRD) analysis (Figure S1 left panel), while ICP-OES analysis demonstrated the mesh-like structures are composed of yttrium phosphate, with approximately equimolar amounts of phosphorus to yttrium (P/Y) (Figure S1 right panel). Because particle crystallinity plays an important role in the fluorescence emissions of UCNPs,[7] the implication is that the transformation could affect the imaging properties of $NaYF_4$

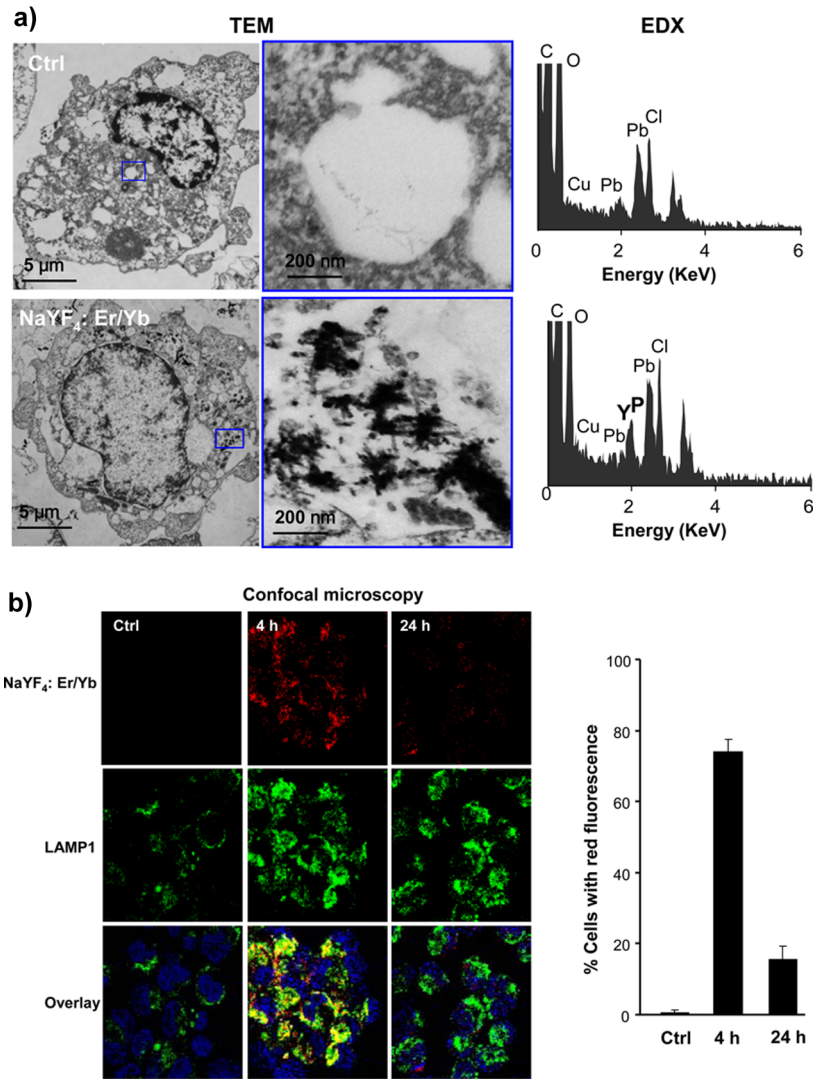

Figure 2. TEM and confocal microscopy to demonstrate particle transformation and quenching of fluorescence intensity of $NaYF_4$ UCNPs in THP-1 cells. (a) Transformation of particles in THP-1 cells as determined by TEM. THP-1 cells were treated with 50 μg/mL UCNPs for 24 h, then fixed and stained to prepare TEM grids. (b) Confocal microscopy imaging of THP-1 cells. After treatment with 25 μg/mL UCNPs for 4 h, THP-1 cells were transferred into UCNP-free media and cultured for 0 or 20 h. The cell samples were collected, fixed, and stained with Alexa Fluor 594 labeled anti-LAMP1 to visualize lysosomes. The percentage of the cells containing particles with red fluorescence was used as a quantitative index to evaluate fluorescence quenching of the UCNPs, taken up into lysosomes.

UCNPs. Indeed, fluorescence spectroscopy showed that PSF treatment was associated with a prominent reduction of the fluorescent intensity of UCNPs, compared to that of the untreated particles (Figure 1).

To determine whether particle transformation and fluorescence quenching of $NaYF_4$:Er/Yb also proceed under biological conditions, a human myeloid cell line, THP-1, was used to study the impact on particle composition and function after uptake in phagolysosomes. As shown by TEM, particle entrance of this acidifying compartment resulted in their transformation into mesh-like structures (Figure 2a). Energy dispersive X-ray spectroscopy (EDX) analysis confirmed the presence of phosphorus in the transformed particles. Assessment of the impact on the imaging capabilities of the UCNPs showed fluorescence quenching of particles taken up by the cells during confocal microscopy (Figure 2b). Thus, while 74% of the cells showed dot-like red fluorescent particles co-localizing with LAMP-positive lysosomes by 4 h, the fraction of cells with observable fluorescence decreased to 16% by 24 h. These results demonstrate that the intralysosomal transformation of $NaYF_4$ UCNP is accompanied by a loss of imaging property.

Phosphonate Coating Stabilizes Particle Composition and Imaging. We have previously demonstrated that prior exposure to phosphate at a neutral or physiological pH can suppress subsequent RE particle transformation in an acidic environment.[29] However, the same stabilization could not be achieved when using phosphate treatment of UCNPs under abiotic and biotic conditions (data not shown). We therefore assessed a

TABLE 1. Library of Coating Molecules

	Coating molecules	Full Name	Structure
Small molecule	Citrate	Citrate	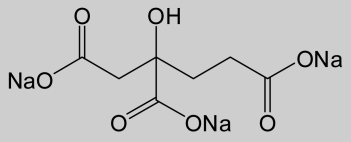
Polymer	PVP	Poly(vinylpyrrolidinone)	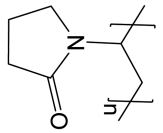
Phosphonate	PMIDA	N-(phosphonomethyl)iminodiacetic acid	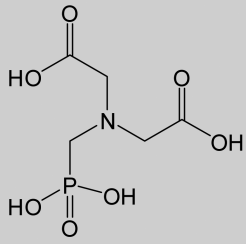
Phosphonate	BPPA	3-Bromopropyl)phosphonic acid	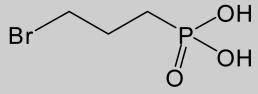
Phosphonate	AMPA	(Aminomethyl)phosphonic acid	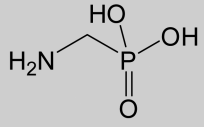
Phosphonate	EDTMP	Ethylenediamine tetra(methylene phosphonic acid)	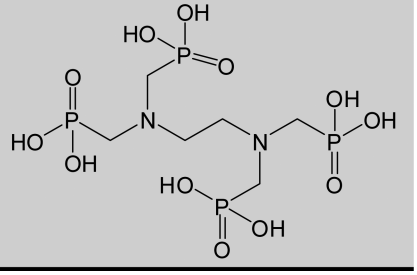

number of phosphonates (PMIDA, BPPA, AMPA, and EDTMP), which represent organophosphorus compounds that contain one or more C-PO(OH)$_2$ or C-PO-(OR)$_2$ groups that can bind to RE atoms on the UCNP surface with high affinity (Table 1). As a control, we also included particles coated with citrate and PVP, which do not contain phosphonate moieties. The schematic in Figure 3a shows the coating procedure. In order to establish the optimal coating efficacy, we used a 0.2−5 weight ratio of phosphonates *vs* particles to determine how this affects the morphological transformation in an acidic PSF environment. This experimentation demonstrated that a weight ratio of 2 was sufficient for effective surface chelation of UCNPs. Comparison of the various coatings demonstrate that while PMIDA, BPPA, PVP, and citrate had minimal protective effects and AMPA provided only marginal improvement, EDTMP was quite effective for comprehensive surface stabilization of $NaYF_4$-based particles (Figures 3b and S2). Moreover, EDTMP also prevented the decay of fluorescence intensity as demonstrated by abiotic fluorescence spectrometry (Figure 3b).

EDTMP-coated particles were comprehensively characterized. As shown in Table S1, the surface charge

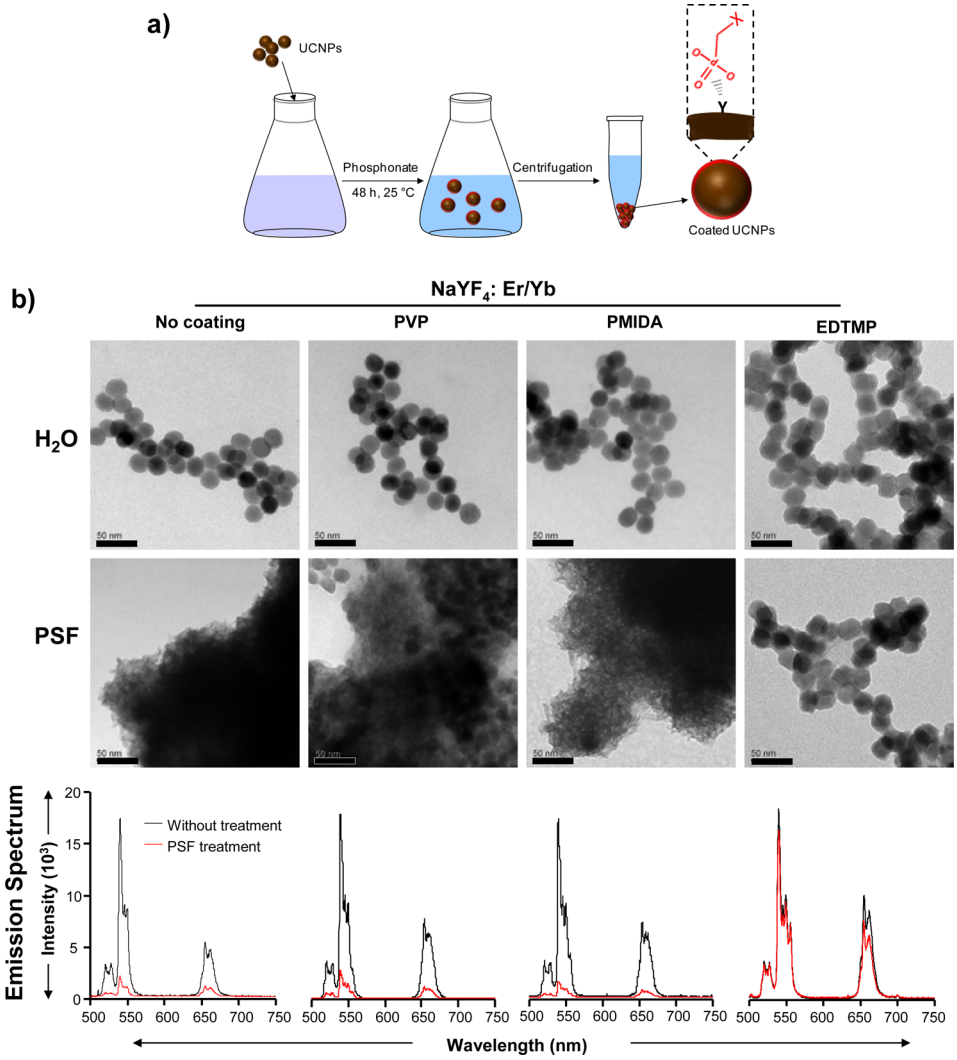

Figure 3. EDTMP coating prevents the transformation and change in emission spectrum of $NaYF_4$: Er/Yb particles. (a) Schematic to explain phosphonate coating. The UCNPs were dispersed in aqueous suspensions for 48 h to react with the coating agents shown in Table 1. Phosphonates bind with high affinity to yttrium atoms on the particle surfaces to form a coating that prevents access of protons to yttrium atoms. (b) TEM and fluorescence emission spectra to compare the altered emission of UCNPs in the absence or presence of three coating agents during PSF exposure. The 200 μg/mL UCNPs were reacted with 400 μg/mL PVP, PMIDA, or EDTMP in DI H_2O for 48 h. The particle pellets were collected by centrifugation, washed three times, and redispersed in DI H_2O at 50 μg/mL and 2 mg/mL, respectively, for TEM and emission spectroscopy. Scale bars are 50 nm.

of these particles changed from +16.4 mV to −11.3 mV in H_2O. There is a similar hydrodynamic size distribution of coated and noncoated particles, yielding values of 28.9 ± 1.0 and 39.2 ± 0.3 nm, respectively (Figure S3 and Table S1). FTIR analysis confirmed the presence of 1095 and 1168 cm^{-1} bands, which are attributed to the antisymmetric and symmetric phosphate stretching vibrations of EDTMP (Figure 4a).[35,36] Moreover, CH_2 stretching bands of 2853 and 2922 cm^{-1}, which are consistent with the presence of oleic acid,[37] were removed during EDTMP coating. The resistance of the EDTMP-coated particles to acidic transformation was confirmed by XRD analysis, which showed that the particles maintained high crystallinity after 24 h in PSF (Figure 4b, left panel). This is confirmed by the maintenance of an identical phosphorus content in the EDTMP-coated particles before and after PSF exposure (Figure 4b, right panel). The schematic in Figure 4c shows the predicted ball-and-stick structure of the EDTMP-RE conjugate, which, as a result of the strong coordination of the phosphonate groups with RE elements, has a high level of resistance against acidic transformation.

In order to determine the biological efficacy of the EDTMP coating, we performed cellular and animal studies. As shown in Figure 5a, the spherical morphology of the internalized EDTMP-$NaYF_4$:Er/Yb particles was preserved in the lysosomes of THP-1 cells, while uncoated particles transformed as described above (Figure 5a). Comparison of the fluorescence imaging intensity of uncoated and EDTMP-coated particles during confocal microscopy showed that while only

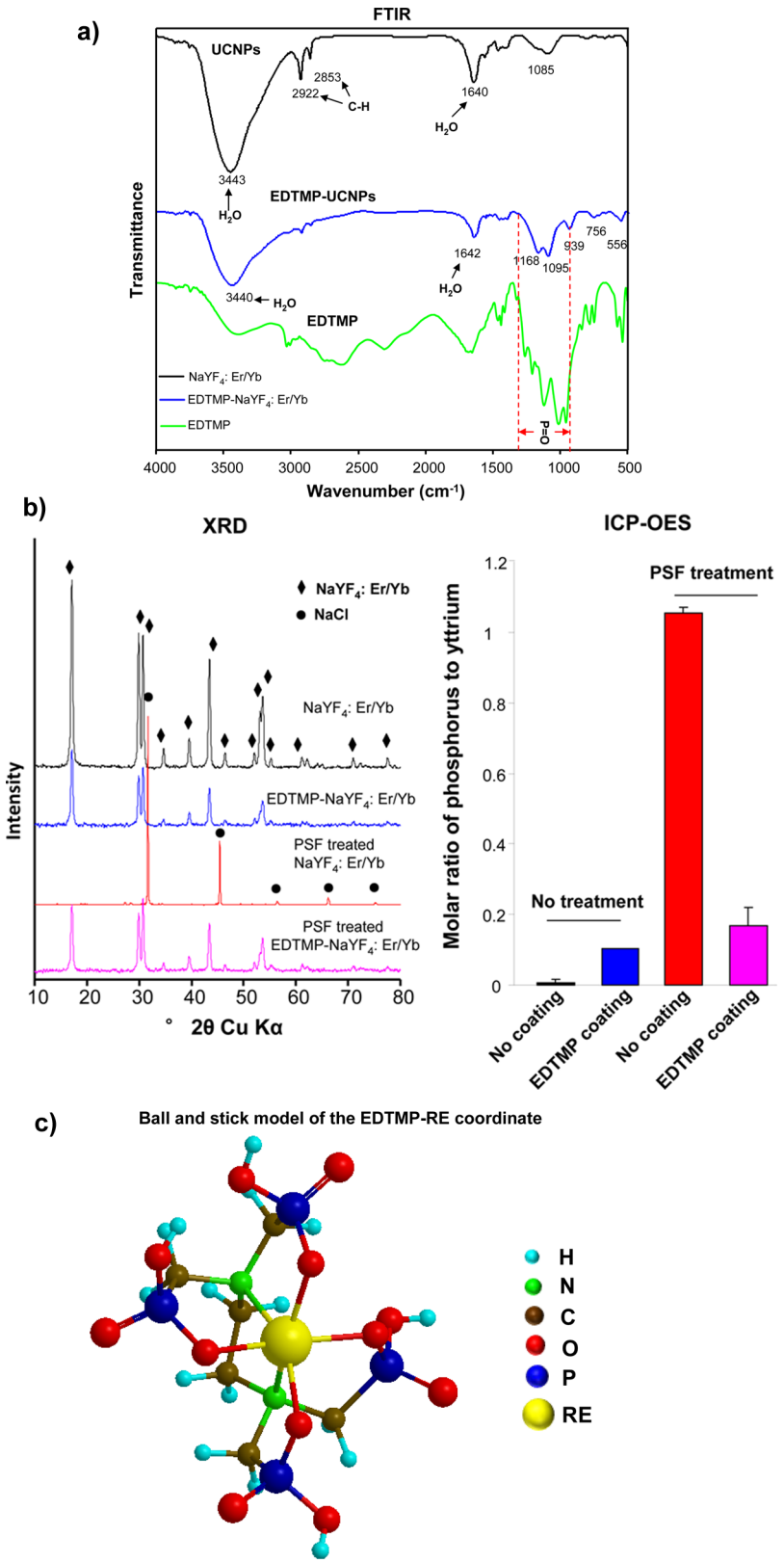

Figure 4. Characterization of $NaYF_4$:Er/Yb particles following EDTMP coating. (a) FTIR spectra of uncoated and EDTMP-coated UCNPs as well as EDTMP by itself. The presence of an EDTMP coating is demonstrated by characteristic P═O peaks. (b) XRD and ICP-OES analysis of uncoated and coated particles before and after PSF treatment. XRD analysis indicates that EDTMP coating protected the crystalline structure and prevented the particle transformation. In contrast, uncoated particles were completely transformed to amorphous YPO_4 during PSF treatment. Quantification of the ratio of yttrium *vs* phosphorus by ICP-OES confirmed the protective effect of EDTMP. (c) Ball-and-stick structure of the EDTMP-RE conjugate. The EDTMP ligand coordinates with the lanthanide atom in a hexadentate structure, which includes two nitrogen and four oxygen atoms linked to a central RE element.

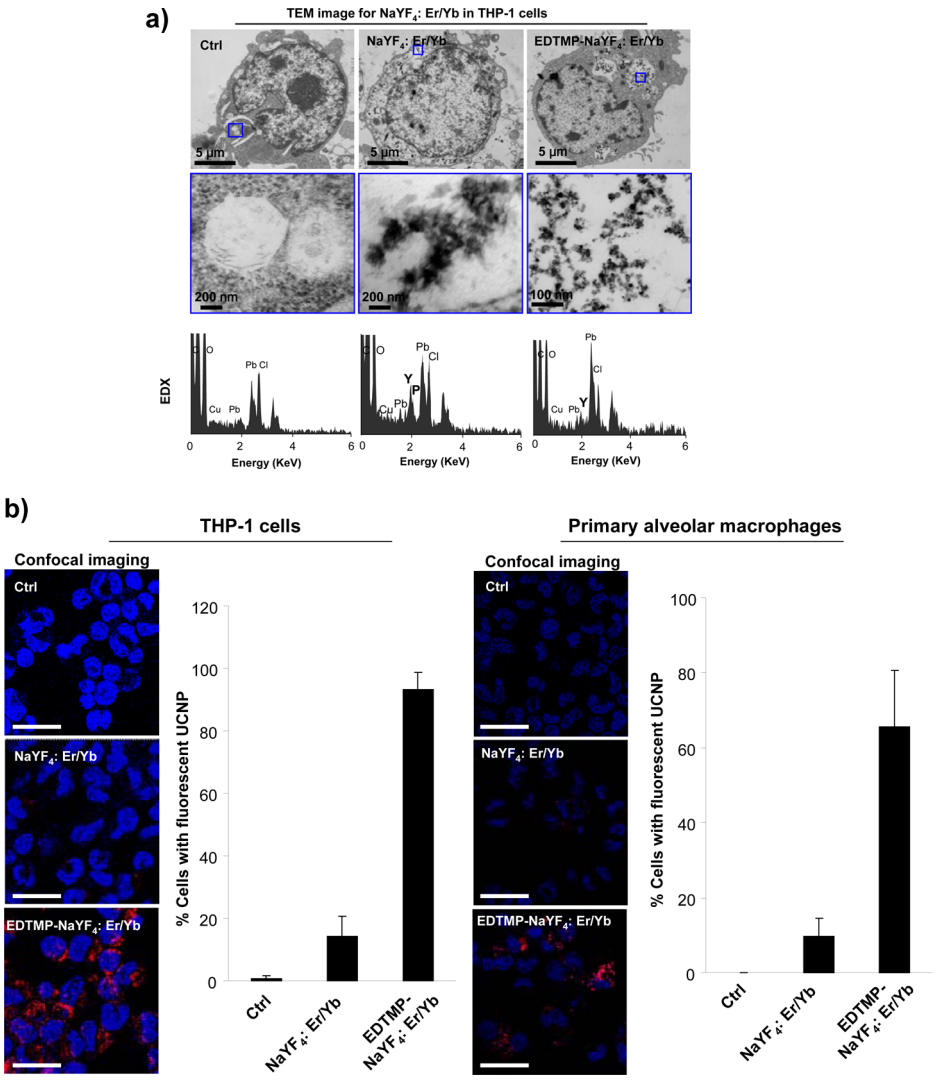

Figure 5. Protective effect of EDTMP coating on $NaYF_4$ UCNP transformation and fluorescence qualities *in vitro* and *in vivo*. (a) TEM imaging to show the uptake and transformation of EDTMP-coated $NaYF_4$ nanoparticles in THP-1 cells. Cells were treated with 50 μg/mL uncoated or EDTMP-coated particles for 24 h. The cells were fixed, stained, and placed on TEM grids. Composition changes were detected by EDX. (b) Imaging of uncoated and coated UCNPs in THP-1 cells and primay alveolar macrophages. THP-1 cells were treated with 25 μg/mL particles for 4 h, followed by 0 or 20 h incubation in UCNP-free media before performance of confocal imaging. Primary alveolar macrophages were obtained from the BALF of mice exposed to 2 mg/kg of uncoated or coated particles for 40 h. Scale bars are 20 μm.

18% of the cells treated with uncoated particles still exhibited fluorescence intensity after 24 h, 92% of cells treated with coated particles remained fluorescent (Figure 5b). In addition, subcutaneous injection of EDTMP-coated and uncoated particles in mice showed that both particle types exhibited bright green fluorescence upon laser excitation of the skin for up to 3 days after injection (Figure S4). However, prior use of PSF exposure before subcutaneous injection demonstrated that only the EDTMP-coated particles could maintain their imaging intensity for the same observation period, while uncoated particles could not be imaged (Figure S4). A similar finding was made when examining pulmonary alveolar macrophages obtained from the bronchoalveolar lavage fluid (BALF) of animals receiving oropharyngeal aspiration of coated and uncoated particles 40 h prior to animal sacrifice. While only 15% of macrophages showed fluorescent particles after mice were treated with uncoated UCNPs, EDTMP-coated UCNPs could be visualized in ~70% of alveolar macrophages, suggesting that coating also maintains particle stability and imaging qualities in the murine lung. These results indicate that EDTMP coating effectively preserves the fluorescence imaging properties of UCNPs *in vitro* and *in vivo*.

EDTMP Coating Prevents the Transformation of Different Types of UCNPs, Regardless of Composition and Shape. In addition to coating of spherical $NaYF_4$-based particles, we also studied the effect of coating on rod-shaped $La(OH)_3$:Er/Yb nanoparticles. After PSF treatment, these particles transformed into urchin-shaped structures, as determined by TEM (Figure 6, left panel). These

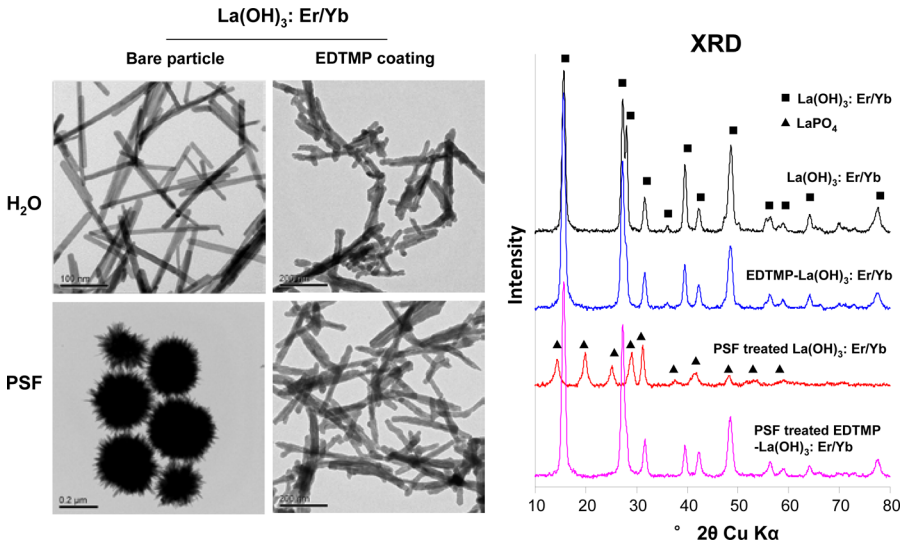

Figure 6. EDTMP coating prevents the transformation of $La(OH)_3$-based nanorods. $La(OH)_3$:Er/Yb nanorods were synthesized by a hydrothermal method as described in the experimental section. Subsequently, 200 μg/mL particles were dispersed in a solution, containing 400 μg/mL EDTMP for 48 h. Coated and uncoated particles were washed and treated in PSF at 100 μg/mL before particle characterization by TEM and XRD.

needlelike structures on the surface were shown by XRD to contain high-crystalline $LaPO_4$ (Figure 6, right panel). However, prior EDTMP coating preserved the rod-shaped structure and crystallinity of the La-based particles. In addition to $NaYF_4$- and $La(OH)_3$-based UCNPs, EDTMP coating also protected a series of Gd-, Eu-, Er-, Nd-, Sm-, Tb-, and Dy-based materials (data not shown).

EDTMP Coating Improves the Biosafety of UCNPs. We have previously shown that the biotransformation of RE nanoparticles triggers lysosomal damage, which leads to NLRP3 inflammasome activation in macrophages and IL-1β release, culminating in pulmonary inflammation and fibrosis.[29,30] In order to determine whether the transformation of UCNPs could elicit similar pro-inflammatory effects, we first performed a confocal study to determine if lysosomes can be damaged by UCNPs; this is accomplished through the use of Magic Red to determine the cellular localization of the lysosomal enzyme cathepsin B.[29] As shown in Figure 7a, untreated cells exhibited a punctate cathepsin B distribution, indicating enzyme containment in intact lysosomes. However, following treatment with uncoated $NaYF_4$ and $La(OH)_3$ UCNPs, damage to the lysosomal membrane leads to the diffuse cytosolic release of cathepsin B, similar to the effect of the positive control, monosodium urate (MSU) crystals. In contrast, THP-1 cells treated with EDTMP-coated particles showed no lysosomal damage (Figure 7a). Since cathepsin B release contributes to the activation of the NLRP3 inflammasome and release of cleaved IL-1β, IL-1β levels were determined by a murine ELISA kit in the supernatant of UCNP-treated THP-1 cells (Figure 7a). While uncoated $NaYF_4$ and $La(OH)_3$ UCNPs could induce dose-dependent cytokine release in the lung, EDTMP-coated particles failed to exert the same effect. EDTMP coating did not impact cell morphology, cell viability (Figure S5), or the cellular uptake of the particles in THP-1 cells (Figure S6).

We also determined whether EDTMP passivation of the UCNP surfaces has an effect on their pro-inflammatory effects in the mouse lung 40 h after oropharyngeal instillation of 2 mg/kg particles. UCNP instillation did not affect the feeding behavior, grooming, or activity of the animals. BALF macrophages were used for *ex vivo* Magic Red staining. Confocal microscopy demonstrated that while uncoated UCNPs could induce cathepsin B release, EDTMP-coated particles did not have the same effect *in vivo* (Figure 7b). Measurement of IL-1β production in the BALF showed that while uncoated particles could induce significant IL-1β production in the lung, EDTMP-coated UCNPs did not elicit a cytokine response (Figure 7b). Most of the inflammatory cells induced by UCNPs are neutrophils (Figure S7). Hematoxylin/eosin (H&E) staining further confirmed that while uncoated particles could induce focal inflammation around small airways, EDTMP-coated UCNPs had no effect (Figure 7c). Both the pristine and EDTMP-coated UCNPs failed to affect PDGF-AA and TGF-β1 production. These data demonstrate that UCNPs coated with EDTMP could serve as a safer design procedure to prevent tissue damage and inflammation.

DISCUSSION

In this study, we demonstrate that RE atoms in UCNPs can lead to particle complexation to cellular phosphate residues, with the possibility to generate a biological hazard as well as interfere in the fluorescence efficiency of these materials. We demonstrate

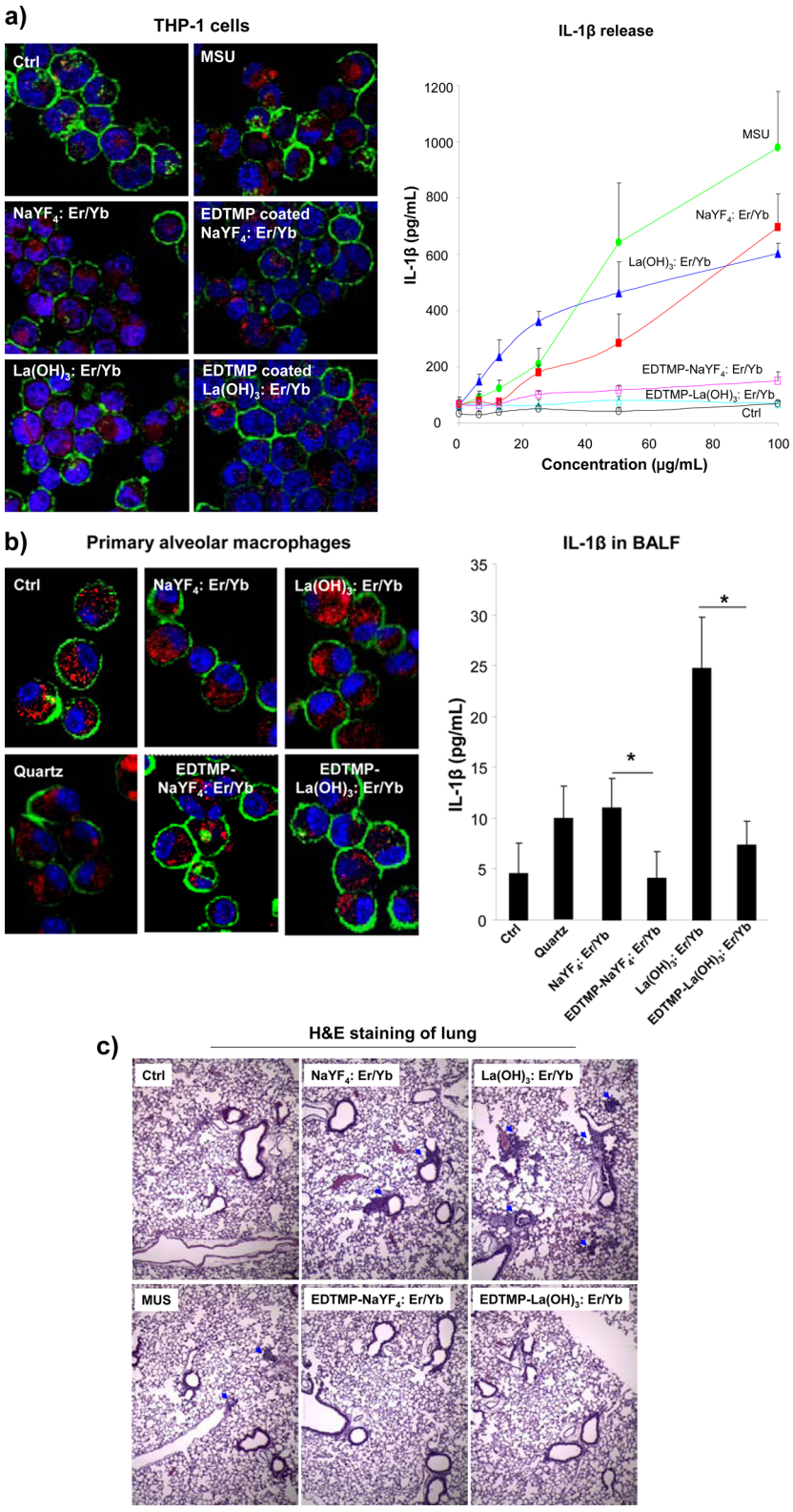

Figure 7. EDTMP coating prevents the pro-inflammatory effects of $NaYF_4$- and $La(OH)_3$-based UCNPs *in vitro* and *in vivo*. (a) Confocal microscopy and ELISA to assess cathepsin B release and IL-1β production, respectively, in THP-1 cells. THP-1 cells were exposed to 50 μg/mL coated or uncoated UCNPs for 6 h, followed by 1 h incubation with the cathepsin B substrate. Cell samples were fixed and stained with Hoechst 33342 and Alexa Fluor 488 conjugated to WGA to observe nuclei and cell membranes, respectively. Supernatants of THP-1 cells, exposed to coated or uncoated particles for 24 h, were collected to determine IL-1β release by ELISA. (b) Confocal microscopy and ELISA to assess cathepsin B release and IL-1β production in pulmonary alveolar macrophages and BALF, respectively. Mice were exposed to 2 mg/kg UCNPs for 40 h. Alveolar macrophages were extracted from BALF and stained with Hoechst 33342 and Alexa Fluor 488-conjugated WGA for confocal imaging. IL-1β production was measured in BALF by ELISA. (c) H & E staining of lung sections from the UCNP-exposed mice.

that UCNP uptake into an acidifying environment, such as the lysosome, leads to the release of RE ions at the particle surface. High-affinity binding to bystander phosphates leads to precipitation of $REPO_4$ on the particle surfaces, leading to transformation into mesh-like or urchin-shaped structures. Moreover, it was demonstrated that this transformation can induce lysosomal damage with cathepsin B release to the cytosol. Subsequent assembly of the NLRP3 inflammasome and IL-1β production can trigger pro-inflammatory effects *in vitro* and *in vivo*. In order to stabilize the UCNP surfaces to prevent phosphate complexation and adverse biological outcomes, we used a series of phosphonates to attempt to achieve surface passivation by high-affinity binding of these organophosphorus groups to RE atoms. Among the phosphonates tested, EDTMP was the most effective in preventing particle transformation under acidic biological conditions, leading to the synthesis of UCNPs that retain their imaging qualities, as well as exhibiting low inflammatory potential in macrophages and the lung. These results demonstrate EDTMP coating could be used as an effective safer design procedure to improve the biological applications of UCNPs.

UCNPs represent a new class of biological luminescence materials that hold several advantages over organic fluorescence probes and semiconductive quantum dots.[20] These advantages include autofluorescence-free signal detection, a high signal-to-noise ratio, narrowband fluorescence emission, large anti-Stokes shift, absence of blinking, long emission lifetimes, and resistance to photobleaching.[38,39] A major finding in this study is that RE-based UCNPs could lose their fluorescence efficiency as a result of intracellular phosphate complexation to particle surfaces. Although the interaction of cellular phosphates with UCNPs has been observed in HeLa cells, no mention was made about physical transformation or an effect on fluorescence efficiency.[40] Although decreases in fluorescence intensity for PEI-, PEG-, or PAA-coated UCNPs have been described in the liver, spleen, lung, or kidney after intravenous injection, these decreases were interpreted as clearance of the injected particles without consideration of physicochemical transformation.[16,23,33] While Cheng *et al*. postulated that decreased fluorescence of intravenous injected UCNPs in the liver could represent particle damage or decomposition, no change in physicochemical composition was demonstrated to explain the findings.[25,33] We demonstrate that UCNP uptake and bioprocessing in the acidic environment of the lysosome leads to a change in particle composition due to $REPO_4$ precipitation on the particle surface, in parallel with altered crystallinity, shape, and size. This leads to increased interatomic spacing of dopants (such as Er and Yb) in the matrix, disrupting their homogeneous distribution and electron transfer and reducing fluorescence efficiency.[7,11,41] It is also worth noting that the physicochemical properties of RE-containing nanomaterials, including composition, size, and shape, could influence the transformation kinetics as well as the ultimate structure of the transformed products. In general, light RE (Sc, La, Ce, Pr, Nd, Pm, Sm, Eu, and Gd) and heavy RE (Y, Tb, Dy, Ho, Er, Tm, Yb, and Lu) materials show different dissolution rates. Gupta *et al*. showed that light RE materials dissolve faster than heavy RE materials in water.[42] This is in agreement with the findings of this study, showing that light RE-based $La(OH)_3$ UCNPs form urchin-shaped structures due to their higher dissolution rates, while the slower dissolution and transformation of heavy RE-based $NaYF_4$ UCNPs result in amorphous, mesh-like structures. In addition, particle shape affects the transformation kinetics. For instance, rod-shaped $La(OH)_3$ is slower to transform than spherical particles, resulting in the formation of large urchin-shaped structures (data not shown).

In addition to the loss of their imaging properties, we found that transformation of UCNPs can lead to the assembly of the NLRP3 inflammasome that has not been demonstrated previously for these particles, which are generally considered as safe for biological use.[33] However, it is known that RE-containing particles can induce pneumoconiosis in miners and polishers, while Gd-based MRI contrast agents can lead to NSF in renal failure patients.[26−29] We recently also demonstrated that the REOs could induce NLRP3 inflammasome activation in macrophages and lung fibrosis in mice.[29] Similar to UCNPs, the mechanism of REO-induced inflammation involves phosphate-induced transformation in the lysosome, leading to damage of the organelle, cathepsin B release, and inflammasome assembly.[29] The mechanism of lysosome damage includes the stripping of structural phosphates from the lipid bilayer, as well as from strategically important phosphoproteins in the cell.[29,30] These processes also control the removal of NLRP3 inflammasomes through autophagosome fusion with the lysosome.[30] The accompanying disruption of autophagic flux and inflammasome accumulation can enhance the pro-inflammatory effects of RE-based nanomaterials.[30] Thus, the prolonged and exaggerated release of IL-1β in the lung can lead to pulmonary fibrosis.[29] Since it is possible that for bioimaging purposes UCNPs may be delivered by intravenous, subcutaneous, peritoneal, or oral routes, additional cell types, organs, and biological processes could be subjected to the effects of UCNPs. Thus, the safer design method that we developed could help to expedite the development of UCNPs for imaging applications.

A variety of approaches may be used to passivate NP surfaces, including coating,[43,44] doping,[45] and encapsulation in a shell structure.[46−49] For the purposes of this study, we chose surface coating, based on the previous observation of suppressing the

physicochemical transformation and pro-inflammatory effects of REOs through prior phosphate interactions under neutral pH conditions.[29] However, this form of coating provides only weak and temporary passivation of REO surfaces, which constitutes the basis for experimenting with organophosphate chelating agents. This led to the identification of EDTMP, which contains four organophosphate groups, as the most effective coating agent to protect against UCNP transformation. The high-affinity binding of EDTMP to the particle surface can be attributed to the unique complexation of lanthanide atoms on the surface. The organophosphate ligand coordinates to the lanthanide atoms in a hexadentate fashion, involving two nitrogen and four oxygen atoms.[50] The tetrahedral phosphonic groups in this complex limit the free space around the central RE atoms, which are shielded from interacting with ligands such as water molecules. As a result, the EDTMP coating is very stable, even under acidic biological conditions. Interestingly, EDTMP can also effectively chelate divalent metal ions, including Co^{II}, Fe^{II}, Zn^{II}, and Cu^{II}.[51,52] It is possible, therefore, that this phosphonate moiety could also be used effectively to coat the surfaces of transition metal nanoparticles, including highly soluble materials such as ZnO and CuO. In summary, EDTMP could be used as an effective coating agent for RE-containing NPs, providing protection against hazardous interactions with the acidifying intracellular compartments, as well as preventing loss of the fluorescence qualities of UCNPs.

CONCLUSIONS

We demonstrate that UCNPs, irrespective of size, shape, and composition, can transform in acidifying cellular compartments, which leads to a decline in their imaging capabilities as well as generation of pro-inflammatory effects. EDTMP coating could prevent complexation to cellular phosphates, which has the effect of preserving the fluorescence qualities as well as preventing injurious effects in macrophages and the murine lung. The protective effect of EDTMP can be attributed to the strong complexation between EDTMP and lanthanide atoms on the particle surface. Thus, EDTMP coating could be used as an effective safer design method for UCNP biological applications, with the advantage of also preserving imaging properties.

MATERIALS AND METHODS

Materials. *N*-(Phosphonomethyl)iminodiacetic acid hydrate (PMIDA) was purchased from Santa Cruz Biotechnology Inc. (Dallas, TX, USA). (Aminomethyl)phosphonic acid (AMPA), (3-bromopropyl)phosphonic acid (BPPA), poly(vinylpyrrolidone) (PVP, wt 360 000), citrate, erbium(III) chloride (99.99%), lanthanum chloride (99.99%), ytterbium(III) chloride hexahydrate (99.99%), yttrium(III) chloride (99.99%), oleic acid, and PEG-coated $NaYF_4$:Er/Yb UCNPs were purchased from Sigma-Aldrich (St. Louis, MO, USA). We also synthesized $NaYF_4$:2%Er/18%Yb particles in-house by a modified thermolysis method as reported.[52] Ethylenediamine tetra(methylenephosphonic acid) (EDTMP) was purchased from Tokyo Chemical Industry Co. (Chuo-ku, Tokyo, Japan); Magic Red cathepsin B assay kit was purchased from Immunochemistry (Bloomington, MN, USA); Hoechst 33342 and the Alexa Fluor 488 conjugate of wheat germ agglutin (WGA) were purchased from Life Technologies (Grand Island, NY, USA). ELISA kits for detection of murine and human IL-1β were purchased from BD Biosciences (San Jose, CA, USA).

In-House Synthesis of $La(OH)_3$:Er/Yb Nanoparticles. We used a hydrothermal method with minor modification to what was previously reported.[54] In a typical synthesis method, we dissolved 0.97 mmol of lanthanum nitrate hexahydrate ($La(NO_3)_3 \bullet 6H_2O$), 0.01 mM of erbium nitrate pentahydrate ($Er(NO_3)_3 \cdot 5H_2O$), and 0.02 mM of ytterbium nitrate pentahydrate ($Yb(NO_3)_3 \cdot 5H_2O$) in 20 mL of deionized water in a 60 mL high-density polyethylene (HDPE) bottle. In another HDPE bottle, 10 mL of a 10 wt % potassium hydroxide (KOH, ≥85%, Sigma-Aldrich) aqueous solution was prepared. The KOH solution was then rapidly added to the lanthanide solution, and the resulting mixture was vigorously mixed for 5 min before transferring into a Teflon-lined stainless steel autoclave. All reactions were carried out in an electric oven at 200 °C for 16 h under autogenous pressure and static conditions. After the crystallization was complete, the autoclave was immediately cooled in a water bath. The fresh, white precipitate was separated by centrifugation and washed three times with deionized water to remove ionic remnants. The final product was dried at 60 °C overnight under ambient conditions.

Surface Coating. A 4 mg amount of UCNPs was dispersed in 20 mL of DI H_2O containing the coating materials (citrate, PVP, PMIDA, AMPA, BPPA, or EDTMP) at concentrations ranging from 40 to 1000 μg/mL. UCNPs were reacted with these coating molecules for 24 h at room temperature with magnetic stirring. The particle solutions were centrifuged at 100 000 rpm/min for 1 h to collect the particle pellets. After washing with DI H_2O, the coated UCNPs were stored at 4 °C for further characterization and use.

Preparation of UCNP Suspensions in Media. Coated or uncoated UCNPs were suspended in DI H_2O at a concentration of 2 mg/mL as stock solutions. These stock solutions were sonicated for 15 min in a bath sonicator (Branson, Danbury, CT, USA, model 2510; 100 W output power; 42 kHz frequencey). An appropriate amount of each UCNP stock solution was added to cell culture media or PBS to achieve the desired final concentrations. The diluted UCNP suspensions were dispersed using a sonication probe (Sonics & Materials, USA) at 32 W for 15 s before introduction to cultured cells.

Physicochemical Characterization of UCNPs. Transmission electron microscopy (TEM) was carried out on a JEOL 1200 EX instrument (accelerating voltage 80 kV). TEM samples were prepared by placing a drop of the particle suspensions (50 μg/mL in DI H_2O) on the grids and leaving them to air-dry at room temperature. High-resolution transmission electron microscopy (HRTEM) coupled with energy dispersive X-ray spectroscopy (EDX) was used to examine fixed cell samples on a Titan S/TEM (FEI, 300 kV). Powder X-ray diffraction (XRD) spectra were obtained on a Philips X'Pert Pro diffractometer, equipped with Cu Kr radiation. Fourier transform infrared (FTIR) spectra were collected using a Bruker Vertex 70 instrument. Dynamic light scattering and analysis of zeta potential (Brookhaven Instruments Corporation, Holtsville, NY, USA) were performed to determine the hydrodynamic diameter and surface charge in water and cell culture media, as previously described.[29,55] An I ICP-OES (ICPE-9000, Shimadzu, Japan) was used to examine rare earth and phosphorus elements.

Detection of Emission Spectra and Animal Imaging. A Technica MLL-III-980-2w (2 W at 980 nm) laser was utilized as the exciting source for abiotic experiments as well as for animal imaging.[53]

A SAHR 320 spectrograph/monochromator, coupled with a PI-MAX intensified CCD camera from Princeton Instruments, was used to record the fluorescence spectra. Briefly, the UCNP samples were dispersed in H_2O at 2 mg/mL and placed in front of the monochromator and the CCD camera. A 980 nm infrared laser was used for sample excitation and generation of emission spectra. For animal imaging, Balb/c mice were anaesthetized by intraperitoneal injection of 100 μL of 1−2% isoflurane. The hair on the back was shaved by a clipper. Untreated or PSF-treated $NaYF_4$:Er/Yb and EDTMP-$NaYF_4$:Er/Yb particles were subcutaneously injected in the back of the animals at 4 mg/kg (2 mg/kg solution, 50 μL). The animals were placed in the laser field for excitation of the injected UCNPs at 980 nm, followed by imaging.

Cell Culture and IL-1β Detection by ELISA. THP-1 cells obtained from ATCC (Manassas, VA, USA) were cultured in RPMI 1640 medium supplemented with 10% fetal bovine serum at 5% CO_2 and 37 °C. Before exposure to UCNPs, aliquots of 5×10^4 cells were primed by seeding in 0.1 mL of medium with 1 μg/mL phorbol 12-myristate acetate overnight in 96-well plates (Corning, NY, USA). For cellular exposure, UCNPs were suspended in complete RPMI 1640, supplemented with 10 ng/mL lipopolysaccharide. After 24 h exposure, IL-1β in the supernatants was detected using a human ELISA kit.

Confocal Microscopy Imaging. Leica confocal SP2MP-FLIM and SP2 1P/FCS microscopes were used to visualize UCNP uptake and cathepsin B release, respectively, in THP-1 cells and alveolar macrophages. High-magnification images were obtained under the 63× objective. To visualize UCNPs in cells, THP-1 cells were treated with 25 μg/mL $NaYF_4$:Er/Yb or EDTMP-$NaYF_4$:Er/Yb particles for 4 h, followed by additional incubation for 0−20 h in UCNP-free media. Alveolar macrophages were extracted from C57BL/6 mice receiving coated or uncoated $NaYF_4$ UCNP exposure for 40 h and then seeded in eight-well chambers overnight. Both THP-1 cells and alveolar macrophages were fixed and stained with Hoechst 33342 or Alexa Fluor 594 labeled anti-LAMP1 to visualize nuclei or lysosomes, respectively. For cathepsin B imaging, alveolar macrophages exposed *in vivo* to 2 mg/kg UCNPs for 40 h by oropharyngeal instillation, or THP-1 cells incubated with 50 μg/mL particles for 6 h, were stained with fluorogenic cathepsin B substrate, using a Magic Red cathepsin B kit. Cells were fixed and stained with Hoechst 33342 and an Alexa Fluor 488 conjugate of WGA to observe nuclei and cell membranes, respectively.

Murine Exposure to UCNPs for Safety Test. Male C57Bl/6 mice (8 weeks old) were purchased from Charles River Laboratories (Hollister, CA, USA) to test the safety of UCNPs. Standard laboratory conditions were used for animal housing as per UCLA guidelines as well as the NIH Guide for the Care and Use of Laboratory Animals (DHEW78-23).[55] Animals were exposed to UCNPs using an oropharyngeal aspiration procedure as described by us.[55] Briefly, animals were anesthetized by intraperitoneal injection of ketamine (100 mg/kg)/xylazine (10 mg/kg) in a total volume of 100 μL and held in a vertical position. Aliquots of 50 μL of UCNP suspensions in PBS were instilled at the back of the tongue to allow pulmonary aspiration of a final dose of 2 mg/kg. Crystalline silica (Min-U-Sil), at a dose of 5 mg/kg, was used as a positive control. Animals were sacrificed after 40 h to collect BALF and lung tissues. IL-1β production was measured in the BALF by ELISA. Lung tissue was stained with hematoxylin/eosin (H&E) for histological evidence of inflammation.

Statistical Analysis. Results were expressed as mean ± SD of multiple determinations from at least three separate experiments. Statistical analysis was performed by one-way ANOVA or Student's *t* test. The difference is regarded statistically significant with $p < 0.05$.

Conflict of Interest: The authors declare no competing financial interest.

Acknowledgment. This work was primarily supported by the National Institute of Environmental Health Sciences, R01 ES016746. The study also leveraged the support provided by the National Science Foundation and the Environmental Protection Agency under Cooperative Agreement Numbers DBI 0830117 and 1266377 and the JCCC grant P30 CA016042. Any opinions, findings, and conclusions or recommendations expressed in this material are those of the authors and do not necessarily represent the views of the National Science Foundation, the Environmental Protection Agency, or the National Institutes of Health.

Supporting Information Available: The hydrodynamic size, zeta potential, XRD spectra, and phosphorus ratio of EDTMP-coated and uncoated $NaYF_4$ UCNPs, TEM images and fluorescence spectra of citrate-, BPPA-, and AMPA-coated $NaYF_4$ UCNPs after PSF treatment, fluorescence images of $NaYF_4$ UCNPs in mice, MTS assay, and cellular uptake of coated and uncoated UCNPs. This material is available free of charge *via* the Internet at http://pubs.acs.org.

REFERENCES AND NOTES

1. Liu, C.; Hou, Y.; Gao, M. Are Rare-Earth Nanoparticles Suitable for in *Vivo* Applications? *Adv. Mater.* **2014**, *26*, 6922–6932.
2. Zhou, J.-C.; Yang, Z.-L.; Dong, W.; Tang, R.-J.; Sun, L.-D.; Yan, C.-H. Bioimaging and Toxicity Assessments of Near-Infrared Upconversion Luminescent $NaYF_4$:Yb,Tm Nanocrystals. *Biomaterials* **2011**, *32*, 9059–9067.
3. Deutsch, Z.; Neeman, L.; Oron, D. Luminescence Upconversion in Colloidal Double Quantum Dots. *Nat. Nanotechnol.* **2013**, *8*, 649–653.
4. Yan, B.; Boyer, J. C.; Habault, D.; Branda, N. R.; Zhao, Y. Near Infrared Light Triggered Release of Biomacromolecules from Hydrogels Loaded with Upconversion Nanoparticles. *J. Am. Chem. Soc.* **2012**, *134*, 16558–16561.
5. Zhang, F.; Braun, G. B.; Pallaoro, A.; Zhang, Y.; Shi, Y.; Cui, D.; Moskovits, M.; Zhao, D.; Stucky, G. D. Mesoporous Multifunctional Upconversion Luminescent and Magnetic "Nanorattle" Materials for Targeted Chemotherapy. *Nano Lett.* **2012**, *12*, 61–67.
6. Gamelin, D. R.; Gudel, H. U. Upconversion Processes in Transition Metal and Rare Earth Metal Systems. *Top. Curr. Chem.* **2001**, *214*, 1–56.
7. Wang, F.; Han, Y.; Lim, C. S.; Lu, Y.; Wang, J.; Xu, J.; Chen, H.; Zhang, C.; Hong, M.; *et al.* Simultaneous Phase and Size Control of Upconversion Nanocrystals through Lanthanide Doping. *Nature* **2010**, *463*, 1061–1065.
8. Auzel, F. Upconversion and Anti-Stokes Processes with F and D Ions in Solids. *Chem. Rev.* **2004**, *104*, 139–173.
9. Liu, C.; Gao, Z.; Zeng, J.; Hou, Y.; Fang, F.; Li, Y.; Qiao, R.; Shen, L.; Lei, H.; *et al.* Magnetic/Upconversion Fluorescent $NaGdF_4$:Yb,Er Nanoparticle-Based Dual-Modal Molecular Probes for Imaging Tiny Tumors *in Vivo*. *ACS Nano* **2013**, *7*, 7227–7240.
10. Liu, Q.; Sun, Y.; Yang, T. S.; Feng, W.; Li, C. G.; Li, F. Y. Sub-10 nm Hexagonal Lanthanide-Doped Naluf4 Upconversion Nanocrystals for Sensitive Bioimaging *in Vivo*. *J. Am. Chem. Soc.* **2011**, *133*, 17122–17125.
11. Wang, F.; Liu, X. G. Recent Advances in the Chemistry of Lanthanide-Doped Upconversion Nanocrystals. *Chem. Soc. Rev.* **2009**, *38*, 976–989.
12. Liu, Q.; Yang, T. S.; Feng, W.; Li, F. Y. Blue-Emissive Upconversion Nanoparticles for Low-Power-Excited Bioimaging *in Vivo*. *J. Am. Chem. Soc.* **2012**, *134*, 5390–5397.
13. Chan, E. M.; Han, G.; Goldberg, J. D.; Gargas, D. J.; Ostrowski, A. D.; Schuck, P. J.; Cohen, B. E.; Milliron, D. J. Combinatorial Discovery of Lanthanide-Doped Nanocrystals with Spectrally Pure Upconverted Emission. *Nano Lett.* **2012**, *12*, 3839–3845.
14. Wang, Y.-F.; Liu, G.-Y.; Sun, L.-D.; Xiao, J.-W.; Zhou, J.-C.; Yan, C.-H. Nd^{3+}-Sensitized Upconversion Nanophosphors: Efficient *in Vivo* Bioimaging Probes with Minimized Heating Effect. *ACS Nano* **2013**, *7*, 7200–7206.
15. Punjabi, A.; Wu, X.; Tokatli-Apollon, A.; El-Rifai, M.; Lee, H.; Zhang, Y.; Wang, C.; Liu, Z.; Chan, E. M.; *et al.* Amplifying the Red-Emission of Upconverting Nanoparticles for Biocompatible Clinically Used Prodrug-Induced Photodynamic Therapy. *ACS Nano* **2014**, *8*, 10621–10630.

16. Chatteriee, D. K.; Rufalhah, A. J.; Zhang, Y. Upconversion Fluorescence Imaging of Cells and Small Animals Using Lanthanide Doped Nanocrystals. *Biomaterials* **2008**, *29*, 937–943.
17. Zhou, J.; Liu, Z.; Li, F. Y. Upconversion Nanophosphors for Small-Animal Imaging. *Chem. Soc. Rev.* **2012**, *41*, 1323–1349.
18. Liu, J. N.; Liu, Y.; Bu, W. B.; Bu, J. W.; Sun, Y.; Du, J. L.; Shi, J. L. Ultrasensitive Nanosensors Based on Upconversion Nanoparticles for Selective Hypoxia Imaging *in Vivo* upon near-Infrared Excitation. *J. Am. Chem. Soc.* **2014**, *136*, 9701–9709.
19. Zhang, Y. H.; Zhang, L. X.; Deng, R. R.; Tian, J.; Zong, Y.; Jin, D. Y.; Liu, X. G. Multicolor Barcoding in a Single Upconversion Crystal. *J. Am. Chem. Soc.* **2014**, *136*, 4893–4896.
20. Maji, S. K.; Sreejith, S.; Joseph, J.; Lin, M.; He, T.; Tong, Y.; Sun, H.; Yu, S. W.-K.; Zhao, Y. Upconversion Nanoparticles as a Contrast Agent for Photoacoustic Imaging in Live Mice. *Adv. Mater.* **2014**, *26*, 5633–5638.
21. Chen, J.; Guo, C.; Wang, M.; Huang, L.; Wang, L.; Mi, C.; Li, J.; Fang, X.; Mao, C.; *et al*. Controllable Synthesis of $NaYF_4$: Yb, Er Upconversion Nanophosphors and Their Application to *in Vivo* Imaging of Caenorhabditis Elegans. *J. Mater. Chem.* **2011**, *21*, 2632–2638.
22. Wang, K.; Ma, J. B.; He, M.; Gao, G.; Xu, H.; Sang, J.; Wang, Y. X.; Zhao, B. Q.; Cui, D. X. Toxicity Assessments of near-Infrared Upconversion Luminescent LaF_3:Yb,Er in Early Development of Zebrafish Embryos. *Theranostics* **2013**, *3*, 258–266.
23. Xiong, L. Q.; Yang, T. S.; Yang, Y.; Xu, C. J.; Li, F. Y. Long-Term *in Vivo* Biodistribution Imaging and Toxicity of Polyacrylic Acid-Coated Upconversion Nanophosphors. *Biomaterials* **2010**, *31*, 7078–7085.
24. Wang, C.; Tao, H. Q.; Cheng, L.; Liu, Z. Near-Infrared Light Induced *in Vivo* Photodynamic Therapy of Cancer Based on Upconversion Nanoparticles. *Biomaterials* **2011**, *32*, 6145–6154.
25. Cheng, L.; Yang, K.; Shao, M. W.; Lu, X. H.; Liu, Z. *In Vivo* Pharmacokinetics, Long-Term Biodistribution and Toxicology Study of Functionalized Upconversion Nanoparticles in Mice. *Nanomedicine* **2011**, *6*, 1327–1340.
26. Schmidt-Lauber, C.; Bossaller, L.; Abujudeh, H. H.; Vladimer, G. I.; Christ, A.; Fitzgerald, K. A.; Latz, E.; Gravallese, E. M.; Marshak-Rothstein, A.; *et al*. Gadolinium-Based Compounds Induce NLRP3-Dependent IL-1beta Production and Peritoneal Inflammation. *Ann. Rheum. Dis.* **2014**, 10.1136/annrheumdis-2013-204900.
27. Prince, M. R.; Zhang, H. L.; Morris, M.; MacGregor, J. L.; Grossman, M. E.; Silberzweig, J.; DeLapaz, R. L.; Lee, H. J.; Magro, C. M.; *et al*. Incidence of Nephrogenic Systemic Fibrosis at Two Large Medical Centers. *Radiology* **2008**, *248*, 807–816.
28. Vocaturo, G.; Colombo, F.; Zanoni, M.; Rodi, F.; Sabbioni, E.; Pietra, R. Human Exposure to Heavy Metals Rare Earth Pneumoconiosis in Occupational Workers. *Chest* **1983**, *83*, 780–783.
29. Li, R.; Ji, Z.; Chang, C. H.; Dunphy, D. R.; Cai, X.; Meng, H.; Zhang, H.; Sun, B.; Wang, X.; *et al*. Surface Interactions with Compartmentalized Cellular Phosphates Explain Rare Earth Oxide Nanoparticle Hazard and Provide Opportunities for Safer Design. *ACS Nano* **2014**, *8*, 1771–1783.
30. Li, R.; Ji, Z.; Qin, H.; Kang, X.; Sun, B.; Wang, M.; Chang, C. H.; Wang, X.; Zhang, H.; *et al*. Interference in Autophagosome Fusion by Rare Earth Nanoparticles Disrupts Autophagic Flux and Regulation of an Interleukin-1β Producing Inflammasome. *ACS Nano* **2014**, *8*, 10280–10292.
31. Saab, G.; Abu-Alfa, A. Nephrogenic Systemic Fibrosis - Implications for Nephrologists. *Eur. J. Radiol.* **2008**, *66*, 208–212.
32. Zou, Z.; Ma, L. Nephrogenic Systemic Fibrosis: Review of 408 Biopsy-Confirmed Cases. *Indian J. Dermatol.* **2011**, *56*, 65–73.
33. Gnach, A.; Lipinski, T.; Bednarkiewicz, A.; Rybka, J.; Capobianco, J. A. Upconverting Nanoparticles: Assessing the Toxicity. *Chem. Soc. Rev.* **2015**, 10.1039/C4CS00177J.
34. Chien, Y. H.; Chou, Y. L.; Wang, S. W.; Hung, S. T.; Liau, M. C.; Chao, Y. J.; Su, C. H.; Yeh, C. S. Near-Infrared Light Photocontrolled Targeting, Bioimaging, and Chemotherapy with Caged Upconversion Nanoparticles *in Vitro* and *in Vivo*. *ACS Nano* **2013**, *7*, 8516–8528.
35. Illy, N.; Couture, G.; Auvergne, R.; Caillol, S.; David, G.; Boutevin, B. New Prospects for the Synthesis of N-alkyl Phosphonate/Phosphonic Acid-Bearing Oligo-Chitosan. *RSC Adv.* **2014**, *4*, 24042–24052.
36. Lu, J.; Li, Y.; Deng, C. Facile Synthesis of Zirconium Phosphonate-Functionalized Magnetic Mesoporous Silica Microspheres Designed for Highly Selective Enrichment of Phosphopeptides. *Nanoscale* **2011**, *3*, 1225–1233.
37. Chen, Q.; Wang, X.; Chen, F.; Zhang, Q.; Dong, B.; Yang, H.; Liu, G.; Zhu, Y. Functionalization of Upconverted Luminescent $NaYF_4$: Yb/Er Nanocrystals by Folic Acid-Chitosan Conjugates for Targeted Lung Cancer Cell Imaging. *J. Mater. Chem.* **2011**, *21*, 7661–7667.
38. Wang, F.; Liu, X. Multicolor Tuning of Lanthanide-Doped Nanoparticles by Single Wavelength Excitation. *Acc. Chem. Res.* **2014**, *47*, 1378–1385.
39. Haase, M.; Schaefer, H. Upconverting Nanoparticles. *Angew. Chem., Int. Ed.* **2011**, *50*, 5808–5829.
40. Jin, J.; Gu, Y.-J.; Man, C. W.-Y.; Cheng, J.; Xu, Z.; Zhang, Y.; Wang, H.; Lee, V. H.-Y.; Cheng, S. H.; *et al*. Polymer-Coated $NaYF_4$:Yb^{3+}, Er^{3+} Upconversion Nanoparticles for Charge-Dependent Cellular Imaging. *ACS Nano* **2011**, *5*, 7838–7847.
41. Schietinger, S.; Menezes, L. d. S.; Lauritzen, B.; Benson, O. Observation of Size Dependence in Multicolor Upconversion in Single Yb^{3+}, Er^{3+} Codoped $NaYF_4$ Nanocrystals. *Nano Lett.* **2009**, *9*, 2477–2481.
42. Gupta, C. K., Krishnamurthy, N. The Rare Earth. In *Extractive Metallurgy of Rare Earths*; Taylor and Francis: Boca Raton, 2004; pp 1−57.
43. Marsico, F.; Turshatov, A.; Pekoz, R.; Avlasevich, Y.; Wagner, M.; Weber, K.; Donadio, D.; Landfester, K.; Baluschev, S.; *et al*. Hyperbranched Unsaturated Polyphosphates as a Protective Matrix for Long-Term Photon Upconversion in Air. *J. Am. Chem. Soc.* **2014**, *136*, 11057–11064.
44. Su, Q. Q.; Han, S. Y.; Xie, X. J.; Zhu, H. M.; Chen, H. Y.; Chen, C. K.; Liu, R. S.; Chen, X. Y.; Wang, F.; *et al*. The Effect of Surface Coating on Energy Migration-Mediated Upconversion. *J. Am. Chem. Soc.* **2012**, *134*, 20849–20857.
45. Duan, P. F.; Yanai, N.; Kimizuka, N. Photon Upconverting Liquids: Matrix-Free Molecular Upconversion Systems Functioning in Air. *J. Am. Chem. Soc.* **2013**, *135*, 19056–19059.
46. Li, X. M.; Zhou, L.; Wei, Y.; El-Toni, A. M.; Zhang, F.; Zhao, D. Y. Anisotropic Growth-Induced Synthesis of Dual-Compartment Janus Mesoporous Silica Nanoparticles for Bimodal Triggered Drugs Delivery. *J. Am. Chem. Soc.* **2014**, *136*, 15086–15092.
47. Sun, Y.; Zhu, X.; Peng, J.; Li, F. Core-Shell Lanthanide Upconversion Nanophosphors as Four-Modal Probes for Tumor Angiogenesis Imaging. *ACS Nano* **2013**, *7*, 11290–11300.
48. Chen, G.; Shen, J.; Ohulchanskyy, T. Y.; Patel, N. J.; Kutikov, A.; Li, Z.; Song, J.; Pandey, R. K.; Agren, H.; *et al*. (alpha-$NaYbF_4$:Tm^{3+})/CaF_2 Core/Shell Nanoparticles with Efficient near-Infrared to near-Infrared Upconversion for High-Contrast Deep Tissue Bioimaging. *ACS Nano* **2012**, *6*, 8280–8287.
49. Zhang, C.; Lee, J. Y. Prevalence of Anisotropic Shell Growth in Rare Earth Core-Shell Upconversion Nanocrystals. *ACS Nano* **2013**, *7*, 4393–4402.
50. Mondry, A.; Janicki, R. From Structural Properties of the Eu-III Complex with Ethylenediaminetetra(Methylenephosphonic Acid) (H8edtmp) Towards Biomedical Applications. *Dalton Trans.* **2006**, 4702–4710.
51. Westerback, S. J.; Martell, A. E. Ethylene-Diamine-Tetra-(Methylene-Phosphonic) Acid. *Nature* **1956**, *178*, 321–322.
52. Motekaitis, R. J.; Murase, I.; Martell, A. E. Equilibriums of Ethylenediamine-N,N,N′,N′-Tetrakis(Methylenephosphonic) Acid with Copper(II), Nickel(II), Cobalt(II), Zinc(II),

Magnesium(II), Calcium(II), and Iron(III) Ions in Aqueous Solution. *Inorg. Chem.* **1976**, *15*, 2303–2306.
53. Dong, J.; Zink, J. I. Taking the Temperature of the Interiors of Magnetically Heated Nanoparticles. *ACS Nano* **2014**, *8*, 5199–5207.
54. Tang, B.; Ge, J. C.; Zhuo, L. H. The Fabrication of $La(OH)_{(3)}$ Nanospheres by a Controllable-Hydrothermal Method with Citric Acid as a Protective Agent. *Nanotechnology* **2004**, *15*, 1749–1751.
55. Li, R.; Wang, X.; Ji, Z.; Sun, B.; Zhang, H.; Chang, C. H.; Lin, S.; Meng, H.; Liao, Y.-P.; *et al*. Surface Charge and Cellular Processing of Covalently Functionalized Multiwall Carbon Nanotubes Determine Pulmonary Toxicity. *ACS Nano* **2013**, *7*, 2352–2368.